Energy 179 (2019) 1094–1102

Contents lists available at ScienceDirect

Energy

journal homepage: www.elsevier.com/locate/energy

A study on thermodynamic and transport properties of carbon dioxide using molecular dynamics simulation

Lei Chen*, Shanyou Wang, Wenquan Tao

Key Laboratory of Thermo-Fluid Science and Engineering, Ministry of Education, School of Energy & Power Engineering, Xi'an Jiaotong University, Xi'an, Shaanxi, 710049, PR China

ARTICLE INFO

Article history:
Received 19 October 2018
Received in revised form
9 May 2019
Accepted 11 May 2019
Available online 16 May 2019

Keywords:
Supercritical carbon dioxide
Molecular dynamics simulation
Radial distribution function
Self-diffusion coefficient

ABSTRACT

Molecular dynamics simulation was applied to test and evaluate the ability of several models of carbon dioxide on predicting thermodynamics and transport properties. Firstly, we compared the liquid-vapor coexist curves of seven kinds of carbon dioxide models by molecular dynamics simulations. It was found that the Cygan_flex model and EPM2 model were more accurate than the others. Then we investigated the structural properties of carbon dioxide using NPT ensemble molecular dynamics simulation. The fluid became less dense with the increasing temperature. Thirdly, the self-diffusion coefficients were studied at temperature and pressure up to 600 K and 80 MPa, respectively. The results showed that the self-diffusion coefficient decreased with the increasing pressure and increased with increasing temperature. Finally, we calculated the thermal conductivity of carbon dioxide at 250 K using EPM2_flex model, Cygan_flex model and TraPPE_flex model. So, we should pay attention to the selection of appropriate carbon dioxide models to obtain different carbon dioxide properties.

© 2019 Elsevier Ltd. All rights reserved.

1. Introduction

Supercritical carbon dioxide Brayton cycle is a more effective way [1] of generating electricity than traditional Rankine cycle. Supercritical carbon dioxide has some excellent properties, having a liquid-like density and gas-like viscosity [2]. As an inert fluid, carbon dioxide could remain chemically stable at ultra-high temperature. This makes it possible to raise vapor temperature entering turbine, typically up to 700 °C [1]. What's more, the critical parameter of carbon dioxide is much lower than water, so it is easy to reach supercritical state. For the purpose of miniaturization of equipment, the whole system of the Brayton cycle needs to operate at a high pressure above 7 MPa [1] to keep the working fluid in supercritical states to maintain high densities. Besides, a supercritical carbon dioxide power system does not have to use equipment for removing oxygen, salt and sewage. Based on these properties, supercritical carbon dioxide is treated as a kind of environment-friendly working fluid.

To be able to detailly know properties of carbon dioxide, a lot of experiments under various conditions would be needed [3]. However, to experiment at high pressure and/or temperature is dangerous, and it's difficult to conduct experiment accurately, what's more, specialized equipment is needed. Furthermore, there are still many variables that need to be investigated. Therefore, experimental research is a complicated work. There exists a way to reduce the amount of experimental work, that is to build an equation of state [4,5] which can extrapolate the existing experimental results. But the EOS method also meets a problem that not all thermal properties can be predicted through equation of state, such as dynamics and structural properties.

Molecular simulation gives another way to study thermodynamics properties [6]. Molecular simulations, such as molecular dynamics and Monte Carlo, have great advantages on predicting properties of fluid at extreme state. With appropriate force field and model [7] which can truly describe the fluid, simulations could be done and various properties [8–10] could be reproduced through statistical mechanical theories, without carrying out expensive, difficult or impossible experiments [11].

Molecular force field is the most important part [12] of molecular dynamics simulation or Monte Carlo simulation [13,14]. A good force field leads to accuracy results. Three ways are available to create a force field. The first way is to obtain the force field parameter from quantum mechanics calculation. In this way, the application range of molecular simulation is expanded. The second

* Corresponding author.
E-mail address: chenlei@mail.xjtu.edu.cn (L. Chen).

https://doi.org/10.1016/j.energy.2019.05.073
0360-5442/© 2019 Elsevier Ltd. All rights reserved.

method is to obtain the force field parameters by fitting the experimental results. This method usually leads to accurate models, but the workload is a bit large. The last way is semiempirical, which partially relies on the experimental results. In 1981, Murthy, Singer, and McDonald [15] proposed a 12-6 Lennard-Jones three-site model of carbon dioxide, known as MSM model, which showed good predictability for various properties. Several later models can be treated as optimization of MSM model, such as EPM, EPM2 [16] and TraPPE [17] models. EPM and EPM2 models were the first attempt to locate the critical point of carbon dioxide by Jonathan and co-workers. Jonathan reported that the critical point calculated using the EPM model was higher than the experimental value, so they improved it and introduced the EPM2 model, which performed well in positioning critical points. These two models were designed to predicting phase properties based on Monte Carlo simulation. TraPPE model was designed to simulate the phase behavior of carbon dioxide too. The models mentioned above are all rigid models whose bond length and angle are fixed, however simulations using flexible models are more convenient to carry out. So, a number of flexible models [18–21] were recently developed based on the rigid ones. Bruin [18] proposed the extended versions of the EPM2 model, namely EPM2_flex model in this study, the shear viscosities under supercritical conditions and along the coexisting line and the thermal conductivity under supercritical conditions were investigated, but a significant difference was still found compared to the reported experimental value. Maginn [19] modified the TraPPE model when studying the ability of ionic liquids for CO2 capture. Also studying carbon dioxide capture, Cygan [20] developed another flexible model, namely Cygan_flex in this study. Maginn [21] did great work on comparing force fields of carbon dioxide and methane in extended temperature range and pressure range. Furthermore, the MBAR technique was applied to improve the accuracy of molecular simulation, decrease calculation uncertainties and reduce the number of simulations required in Maginn's study [21].

In this study, performance of various models of carbon dioxide was investigated. Although these models were proposed to predict the liquid-vapor properties, they could be extended to predict other thermodynamic properties. In the first part of this study, we performed molecular dynamics simulations to test their performance on probing liquid-vapor interfacial properties, using MSM, EPM, EPM2, TraPPE, EPM2_flex, Cygan_flex and TraPPE_flex models. In the second part, the structural property was studied. Part three introduced the dynamics characters. Only EPM2 model was considered in the second and third part of this paper. In the last part, non-equilibrium molecular dynamics simulation was adopted to evaluate thermal conductivity of carbon dioxide, and in this part three flexible models were studied, EPM2_flex, Cygan_flex and TraPPE_flex models.

2. Simulation methods and details

Classical molecular dynamics simulations were performed using LAMMPS in the present study. In the first part of this work, we studied the liquid-vapor interfacial characters [22] by performing equilibrium NVT calculations, and the critical point could be got through fitting the liquid-vapor interfacial thickness curve. After that, another simulation box was built to calculate the structural properties. And then, NPT simulations were carried out to investigate the dynamics properties. Finally, non-equilibrium simulations were performed to study the thermal conductivity of carbon dioxide.

2.1. Force field

Lennard-Jones potential is the most popular model for approximating the van der Waals interaction between a pair of atoms. The standard 12-6 Lennard-Jones potential was used in this paper, which is given by:

$$E(r_{ij}) = 4\varepsilon\left[\left(\frac{\sigma_{ij}}{r_{ij}}\right)^{12} - \left(\frac{\sigma_{ij}}{r_{ij}}\right)^{6}\right] \tag{1}$$

where ε is the depth of the potential well which indicates the strength of the interaction, r_{ij} means the distance between two atoms, σ_{ij} represents the finite distance at which the inter-particle potential is zero, and the r_{ij}^{-12} term is the repulsive term, r_{ij}^{-6} is the attractive term. Through this potential equation, the inter-particle potential energy could be calculated as $E(r_{ij})$. Additionally, Lorentz–Berthelot mixing method was used to get the force field parameter for interactions between different types of particles.

As for the Coulombic pairwise interaction, we employed atom based partial charge model, and calculated the Coulombic interaction using:

$$E_Q(r_{ij}) = \frac{Cq_iq_j}{\varepsilon r_{ij}} \tag{2}$$

where C is an energy-conversion constant, q_i and q_j are the charges of 2 atoms, and ε is the dielectric constant.

In this work, seven three-site models of carbon dioxide were involved, including four rigid models and three flexible models. Four rigid models, namely EPM model, EPM2 model [16], MSM model [15] and TraPPE [17] model, all have fixed bond length and angle. As for three flexible models, namely EPM2_flexmodel [18], Cygan_flex model [20] and TraPPE_flex [19] model, the bonds can be stretched and the angle can be bent. The force field parameters for each model are listed in Table 1.

For the rigid models, only inter-atom energy is considered because the bond and angle are rigid. As for the flexible models, not only inter-atom energy but also intra-molecule energy is considered. Intra-molecule energy terms could be calculated by harmonic functions:

$$E_{bond} = \frac{1}{2}k_{bond}(r - r_0)^2 \tag{3}$$

$$E_{angle} = \frac{1}{2}k_{angle}(\theta - \theta_0)^2 \tag{4}$$

where r_0 and θ_0 indicate the equilibrium configuration of the molecule, k_{bond} and k_{angle} are the energy constants. If the configuration of the molecule is changed by external forces, the intra-molecule potential energy will increase.

2.2. Simulation details

Firstly, a $40 \times 40 \times 150(\text{Å}^3)$ rectangular simulation box was built to study the interfacial characters. 640 carbon dioxide molecules were placed in the middle slab of the box regularly and two vacuum layers located next to carbon dioxide layer to form a sandwich. Periodic boundary conditions were applied in all three directions. The original configuration was unstable, so the first step must be equilibrium-run to make the system stable and 5 ns for equilibrium run. After getting equilibrium state, 1 ns MD simulation for statistic calculation was needed. In this part, NVT ensemble was always employed.

Secondly, a cubic simulation box was built to study the structural properties and dynamics properties of carbon dioxide. Because of the sensitivity of self-diffusion coefficient to system size,

Table 1
Force field parameters for each model used in this work.

		EPM	EPM2	MSM	TraPPE	EPM2_flex	Cygan_flex	TraPPE_flex
ε /Kcal· mol^{-1}	C–C	0.0576	0.0558	0.0576	0.0536	0.0558	0.0559	0.0536
	O–O	0.1648	0.1599	0.1651	0.1569	0.1599	0.1596	0.1569
σ_{ij} /Å	C–C	2.785	2.757	2.790	2.800	2.757	2.800	2.800
	O–O	3.064	3.033	3.010	3.050	3.033	3.028	3.050
r_0 /Å	C–O	1.161	1.149	1.160	1.160	1.149	1.162	1.160
θ_0 /°	–	180	180	180	180	180	180	180
k_{bond} /Kcal· mol^{-1}· Å^{-2}	–	–	–	–	–	2565.547	2017.033	2057.096
k_{angle} /*Kcal*· *mol*$^{-1}$· *rad*$^{-2}$	–	–	–	–	–	295.2804	107.9589	111.9509
q_e /*e*	C	+0.6645	+0.6512	+0.596	+0.7	+0.6512	+0.6512	+0.7

a large enough system was built in this part, which contained 1728 molecules. Periodic boundary condition was still needed. And NPT simulation was operated in this part.

Finally, this study compared the performance of three models on predicting thermal conductivity. Both equilibrium molecular dynamics simulation [23] and non-equilibrium molecular dynamics simulation [24] have method for measuring thermal conductivity of fluid. The present work employed a kind of non-equilibrium method, namely Langevin thermostating technique [9,25]. For this simulation, the volume of the simulation box was a constant, so the number of molecules added into the box should match the density of carbon dioxide under the simulation condition. The size of the simulation box was $200 \times 30 \times 30(\text{Å}^3)$ with periodic boundary conditions. The original configuration of the system was constructed by placing the molecules randomly. To stabilize the system, 200 ps NVT run and 2 ns NVE run were needed. After the system reached thermal equilibrium, a 5 ns non-equilibrium molecular dynamics simulation was performed in microcanonical ensemble (NVE). In particular, during the 5 ns calculation run, a hot slab and a cold slab should be thermostated respectively.

3. Results and discussion

3.1. Density profile and liquid-vapor interface

Firstly, we focused on the density profile and predicted the liquid-vapor interfacial properties [26,27]. We built simulation boxes for seven models and ran simulations at temperature of 230–300 K, respectively. The snapshots of interfaces at different temperature are shown in Fig. 2, and the simulation results of Cygan_flex model are taken as example, the results of other models are similar to this. From Fig. 2, the interfaces between liquid phase and vapor phase could be visually observed. What's more, the region where the molecules are dense indicates liquid phase, and the region where the molecules are sparse represents vapor phase. As the temperature increases, the number of molecules in the vapor phase increases, and the number of molecules in liquid phase decreases.

To quantitatively study density changes near the liquid-vapor interface, the density was considered as a function of z-position. Therefore, the simulation box was divided into 300 slabs along z direction. And the density of carbon dioxide in each slab was calculated at equilibrium state. For comparison, we adjusted the z-coordinate and the results for each model at different temperatures are shown below. Fig. 3 shows the density distribution of seven models. It is easy to find the vapor phase, liquid phase and the location of the interface. The accuracy can be controlled by increasing or decreasing the total number of molecules and the size of simulation system, but increasing the simulation system will increase the time cost of the simulation, so we selected a small simulation system on the premise of ensuring the accuracy.

The average densities of gas phase and liquid phase were calculated to represent liquid density and vapor density respectively. Through these densities at different temperature, the coexistence curve can be draw, as shown in Fig. 4. The liquid-vapor coexistence curve obtained in this study was compared with the NIST data. The Cygan_flex model and EPM2 model are more accurate models, but the TraPPE model and TraPPE_flex model are the inaccurate models for predicting density below critical temperature. Table 2 compared the simulation results for the liquid-vapor equilibrium obtained with the EPM2 model and Cygan_flex model with NIST data. In NVT ensemble simulation, all models performed very well in liquid phase, but the results of vapor densities were not very good.

As shown in Fig. 3, the liquid-vapor interface is continuous. The thickness of the interface is an important parameter to describe the liquid-vapor interface. It is usually not easy to determine the thickness of the liquid-vapor interface by macro-method, because

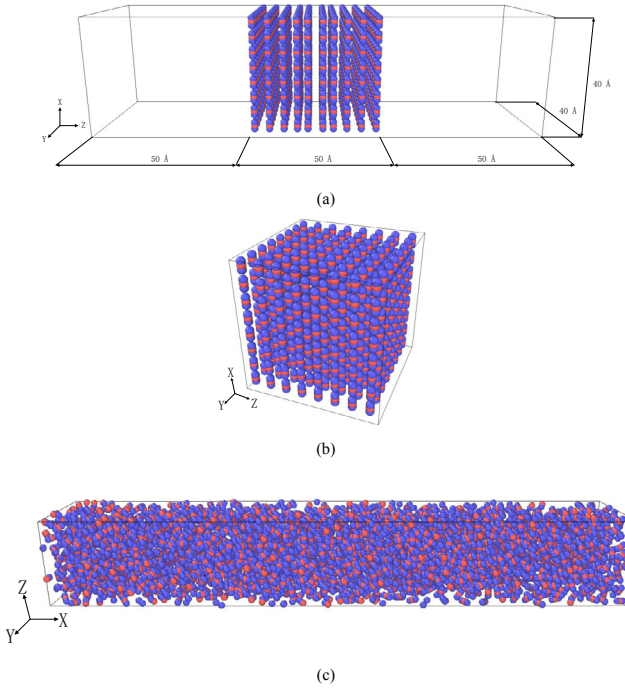

Fig. 1. Snapshots of the original structures. (a) The simulation box for studying liquid-vapor interfacial characters; (b) the simulation box for studying structural and dynamics properties; (c) the simulation box for studying thermal conductivity.

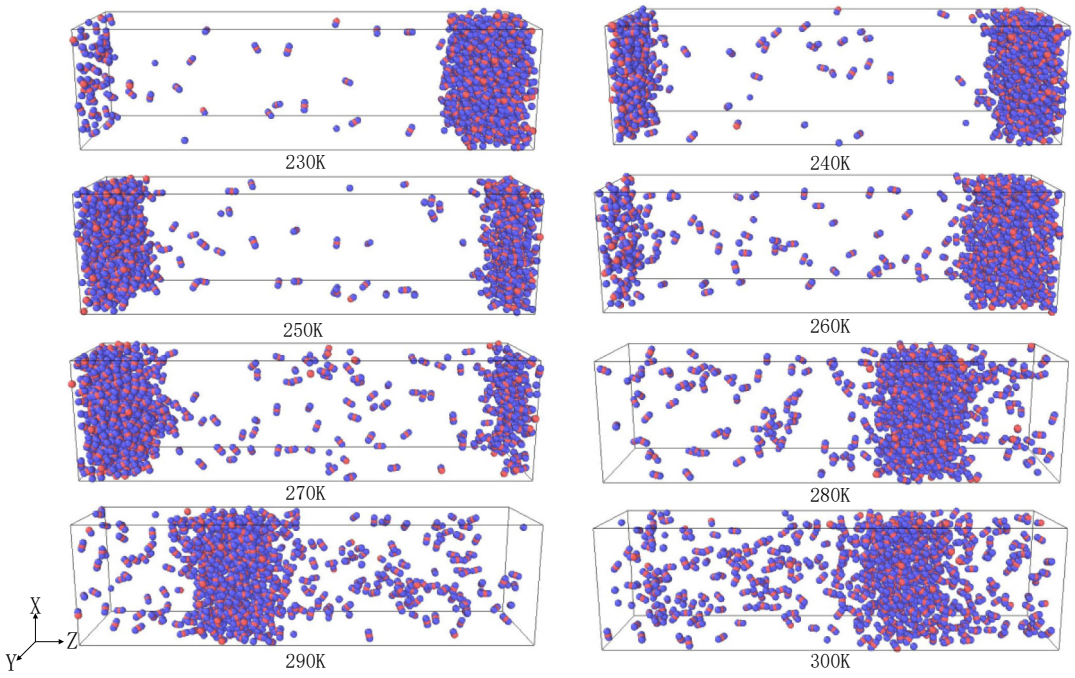

Fig. 2. Snapshots of interfaces at different temperatures (Cygan_flex model).

the liquid-vapor interface is a transition zone between two phases, and it is an ultra-thin region with thickness of a few nanometers. In the present work, we employed "15–85" rule [28] to determine the thickness of liquid-vapor interface. The so called "15–85" rule actually determines the density range of the liquid-vapor interface.

$$\rho_v + \frac{15}{100}(\rho_l - \rho_v);\ \rho_v + \frac{85}{100}(\rho_l - \rho_v) \tag{5}$$

Through "15–85" rule, we measured the thickness of liquid-vapor interface at each temperature we studied, and the results are shown in Fig. 5. It is obvious that the interfacial thickness will increase with the temperature. Theoretically, the interfacial thickness will increase to infinity if the temperature reaches the critical point. But in this study, although the temperature is very close to the actual critical temperature, the interfacial thickness does not increase rapidly. It seems that all seven models involved in this study underrate the interfacial thickness, which means they overestimate the critical temperature.

When the temperature is treated as a function of the reciprocal of interfacial thickness, it will become a linear curve, and the vertical intercept of the curve indicates the predicted critical temperature. Table 3 shows the predicted critical temperature of each model. Although the predicted values of these models through NVT ensemble molecular dynamics simulation are not particularly good, they perform well in other Monte Carlo molecular simulation. What we did in the present work introduce the characters of liquid-vapor interface qualitatively.

3.2. Radial distribution function

The structure profile of carbon dioxide was also discussed in this study. The radial distribution function was used to describe how density varies as a function of the distance from the reference particle. For an isotropic system, if a given particle is set as a reference and the average density of the target particle is ρ, the local density of target particle at a distance of r from the reference would be $\rho g(r)$, where $g(r)$ is the radial distribution function. Formula 6 is used to calculate the radial distribution function, where V means the volume of the system, N is the total number of the target particle in the system, $n(r)$ indicates the number of target particles in the shell at the distance r from the reference particle, $4\pi r^2 dr$ represents the volume the shell.

$$g(r) = \frac{V}{N}\frac{n(r)}{4\pi r^2 dr} \tag{6}$$

Radial distribution function is a usual structural property we could get from molecular dynamics simulation, and this profile could be verified with experimental results from neutron-diffraction or X-ray experiments [29–31].

The structure properties of carbon dioxide have been researched through experiments, but different authors may get different results because of the uncertainty and statistical fluctuation. Former researchers introduced the concept of intermolecular radial distribution function, which is actually a weighted sum of partial radial distribution functions. The so-called neutron weighed radial distribution function for carbon dioxide is shown as formula 7. In formula 7, $g_{C-C}(r)$, $g_{C-O}(r)$ and $g_{O-O}(r)$ mean the partial atom-atom radial distribution functions [30,32].

$$g_m(r) = 0.133 g_{C-C}(r) + 0.464 g_{C-O}(r) + 0.403 g_{O-O}(r) \tag{7}$$

In this study, the neutron weighted radial distribution function was used to compare the simulated structure property with experiment. We employed EPM2 model to do this comparation with the same state as the reference. Fig. 6 shows great agreement between the present work with former experiment result [31,32] and simulation work [33]. Fig. 6 shows the short-range structure of carbon dioxide at the temperature of 240 K and pressure of 1.3 MPa. It shows that the first peak of C–C pairwise appears at 4.05 (±0.05) Å and the first valley appears at 5.85 (±0.05) Å. We could also get the position of the first peaks of C–O pair and O–O pair, 4.05 (±0.05) Å and 3.15 (±0.05) Å. It should be noticed that the C–O and O–O pairs do not consider the intramolecular pairs. Generally speaking, if the first peak is high and sharp, it means that the atoms

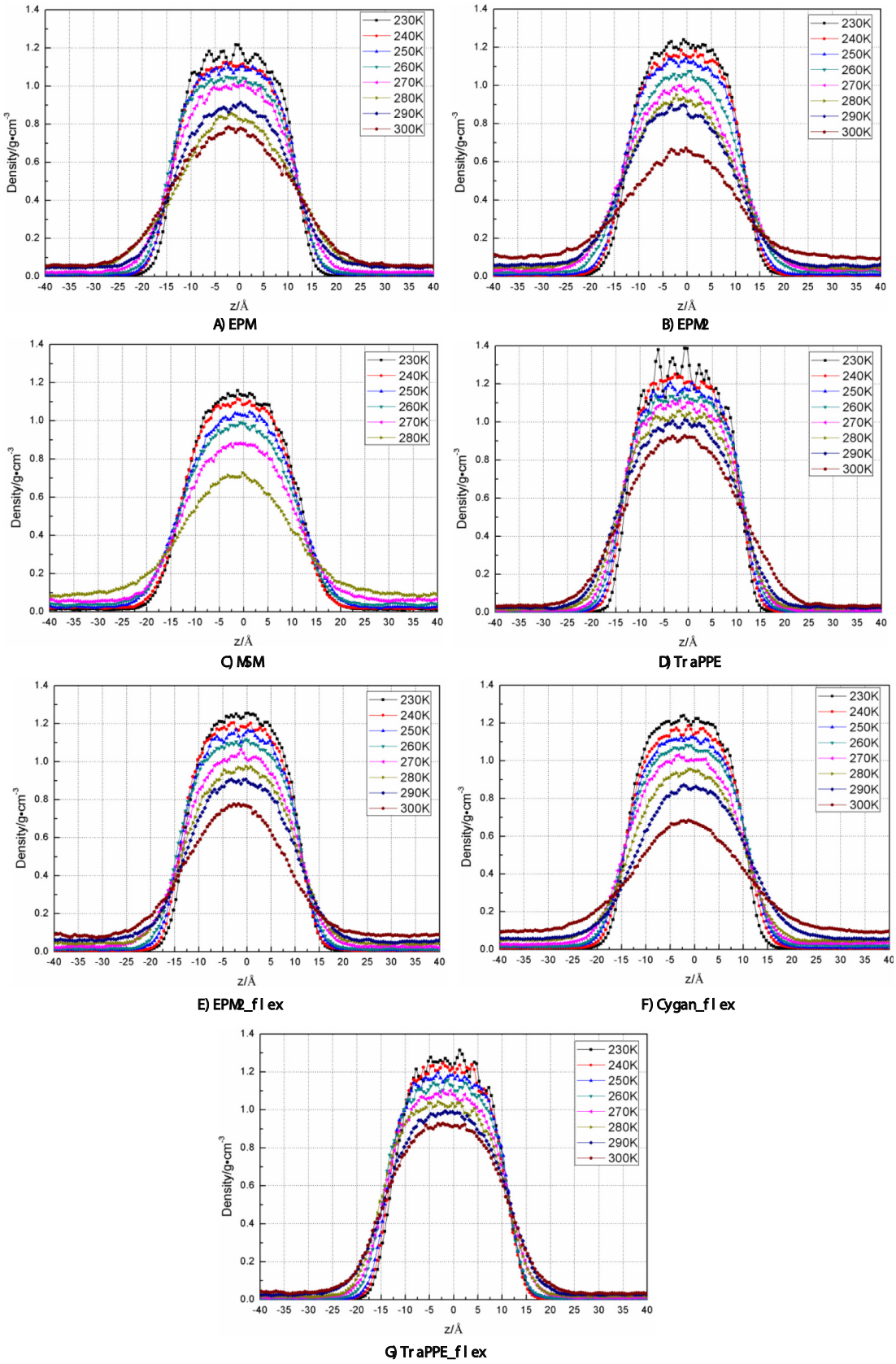

Fig. 3. Density distributions along z-position.

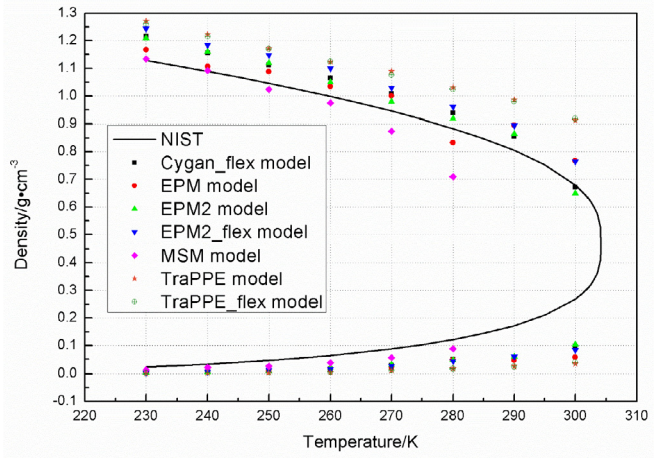

Fig. 4. Liquid-vapor coexistence curve.

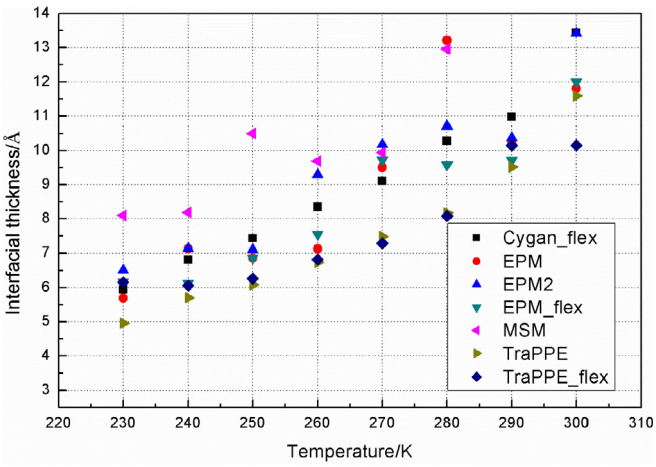

Fig. 5. Relationship between thickness of liquid-vapor interface and temperature.

are tightly bound each other, the arrangement of surrounding atoms is relatively regular, and the distance between the first layer coordination atoms and the central atoms is short.

To investigate the temperature effect on radial distribution function, Fig. 7 shows the partial radial functions with increasing temperature at pressure of 8 MPa. The radial distribution functions clearly indicate the structure loss when the temperature increases. The first peaks of RDFs are broadened and diminished with the increasing temperature. What's more, the second peaks of RDFs disappear by the temperature of 350 K, which means the disorganization of second shell of the reference molecule. We could also observe the shift of the position of the first peak. Indeed, with the increasing temperature the fluid becomes less dense, corresponding to the reduction and shift of the first peak.

3.3. Self-diffusion coefficient

Self-diffusion coefficient [34–38] reflects the intensity of Brownian motion of the molecules. In the present work, Einstein's theory [35] was used to calculate self-diffusion coefficient. Einstein's theory for Brownian motion introduces a formulation of diffusion coefficient, in which the self-diffusion coefficient could be calculated from the mean squared displacement of a Brownian particle, given by:

$$D_s = \frac{1}{6}\lim_{t\to\infty}\frac{d}{dt}\left(\frac{1}{N}\sum_{n=1}^{N}[r_n(t)-r_n(0)]^2\right) \quad (8)$$

In this part, we employed EPM2 model. We measured the self-diffusion coefficients of carbon dioxide in the temperature range of 310 K–600 K and pressure range of 1 MPa–80 MPa.

The results of EPM2 model are show in Fig. 8. It is easy to find that the self-diffusion coefficient of carbon dioxide will decrease with the increase of pressure. When the pressure is low, carbon dioxide is in the superheated state and its density is extremely low. In this case, the fluid is easily compressed and the mean free path of the molecules is large, as a result, the self-diffusion coefficient is pretty high. The self-diffusion coefficient will sharply decrease if the pressure increases, especially near the critical pressure point. When the pressure is higher than 15 MPa, the fluid is in the supercritical state, in which state the density is close to liquid state. Meanwhile, the self-diffusion coefficient is also close to that of liquid carbon dioxide. When the pressure is lower than the critical pressure, the self-diffusion coefficient is sensitive to the pressure change, while when the pressure is higher than the critical pressure, the self-diffusion coefficient is not sensitive to the pressure change.

The self-diffusion coefficient is also affected by temperature. From Fig. 8, we could also observe that the self-diffusion coefficient

Table 2
Comparison of simulation results for the liquid-vapor equilibrium obtained with the EPM2 model and Cygan_flex model with NIST data.

Temperature (K)	Model	Sim. (liquid g·cm^{-3})	Expt. (liquid g·cm^{-3})	Dev (%)	Sim. (vapor g·cm^{-3})	Expt. (vapor g·cm^{-3})	Dev (%)
230	Cygan_flex	1.215	1.1287	7.6	0.00492	0.02327	78.8
	EPM2	1.210		7.2	0.00485		79.2
240	Cygan_flex	1.156	1.0889	6.1	0.00849	0.03329	74.5
	EPM2	1.159		6.4	0.00672		79.8
250	Cygan_flex	1.112	1.046	6.3	0.01577	0.04664	66.2
	EPM2	1.119		6.9	0.01095		76.5
260	Cygan_flex	1.065	0.99889	6.6	0.01637	0.06442	74.6
	EPM2	1.050		5.1	0.02066		67.9
270	Cygan_flex	1.008	0.94583	6.6	0.02785	0.08837	68.5
	EPM2	0.980		3.6	0.03244		63.3
280	Cygan_flex	0.939	0.88358	6.3	0.0511	0.12174	58.0
	EPM2	0.919		4	0.04724		61.2
290	Cygan_flex	0.856	0.80467	6.3	0.05774	0.17196	66.4
	EPM2	0.864		7.5	0.05995		65.1
300	Cygan_flex	0.672	0.67924	1.1	0.09827	0.26858	63.4
	EPM2	0.649		4.4	0.10439		61.1

Table 3
Predicted critical temperature of each model.

	EPM	EPM2	MSM	TraPPE	EPM2_flex	Cygan_flex	TraPPE_flex
Temperature/K	342	355	350	355	360	354	380

will increase with temperature and the increasing rate varies with temperature. When the pressure is extremely high, the self-diffusion coefficient will not increase too much with temperature.

3.4. Thermal conductivity

As mentioned above, we investigated the thermal conductivity of carbon dioxide through non-equilibrium molecular dynamics simulation. Previous researches have reported several non-equilibrium molecular dynamics methods for thermal conductivity calculation, such as swapping particle momentum and heat exchange algorithm [39–42]. But this study chose a most intuitive way named thermostating method. The simulation box is shown in Fig. 1(c), the simulation box was divided into 20 slabs along x-direction firstly, 1 nm thick per slab. These slabs were marked from 1 to 20. And we set the temperature of the 1st slab as T_{hot} and the temperature of 11th slab as T_{cold}, in which condition we could measure the thermal conductivity of carbon dioxide at $T = \frac{1}{2}(T_{hot} + T_{cold})$. It should be noted that the density of carbon dioxide is directly related to the number of molecules in the system, what's more, the pressure of the simulation box is also related to the number of molecules and the temperature. Therefore, in this part, the state of carbon dioxide was controlled by the number of molecules and the simulated temperature. In the whole simulation box, only the hot slab and the cold slab were thermostated, and the temperature of other slabs could be calculated by the molecular kinetic energy. Finally, the temperature distribution along x-direction would be gotten from statistic average data. And then the temperature gradient could be calculated from the temperature distribution. Fourier's law describes how heat flux transports, and the thermal conductivity could be obtained by formula 9.

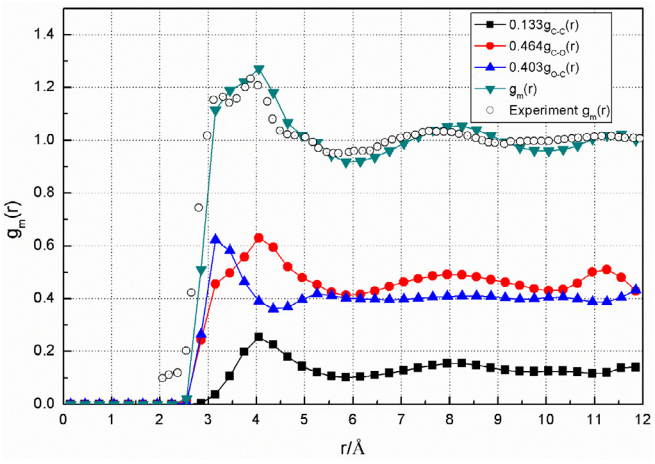

Fig. 6. Radial distribution functions and intermolecular distribution function of the state T = 240 K and P = 1.3 MPa.

$$\lambda = -\frac{\Phi}{A}\frac{dx}{dT} \tag{9}$$

In which, Φ means the heat flux, A is the cross-sectional area of the simulation box perpendicular to the x direction, and $\frac{dT}{dx}$ represents the temperature gradient. The calculation of temperature gradient has been already discussed above. The cross-sectional area is a known structural parameter, and the variable Φ should be measured from thermostating process. The temperature of hot and cold regions was maintained by adding or removing molecular kinetic energy, and the total energy of whole system was unchanged. Therefore, as long as the energy added to hot region was monitored, the thermal conductivity was available. In this section, three models of carbon dioxide were considered, namely EPM2_flex, Cygan_flex and TraPPE_flex.

In this study we constructed 3 simulation systems, which consist of 2600, 2800 and 3000 molecules in the boxes respectively, corresponding to 1.055, 1.137 and 1.218 g /cm^3 systems. Fig. 9 shows the average temperature distribution along x-direction with EPM2_flex model at temperature of 250 K. We obtained similar profiles for Cygan_flex and TraPPE_flex models. The temperature distribution is almost linear in analysis region and the temperature gradient is chosen to be 3–5 K/nm. Fig. 10 shows the density distribution, and we found that the density of cold region was a little higher than the average, meanwhile the density of hot

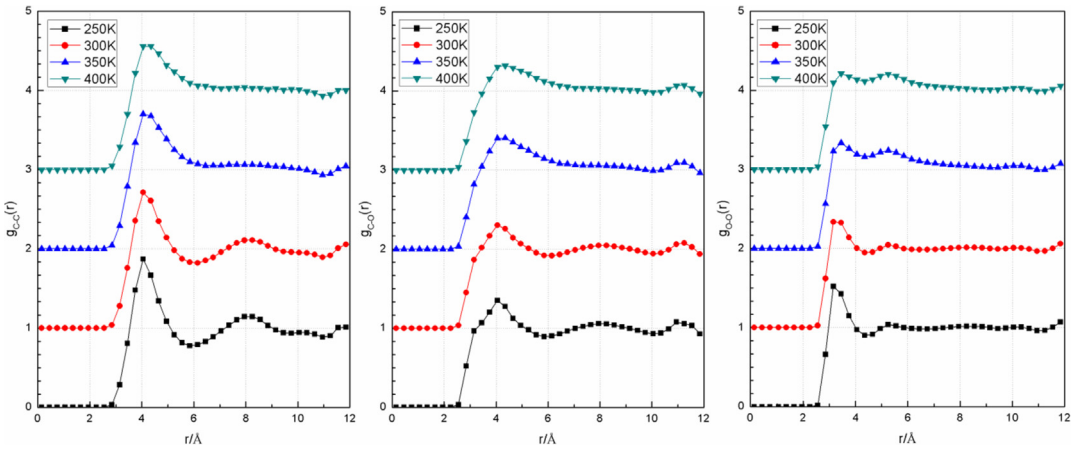

Fig. 7. Partial radial distribution functions at different temperatures.

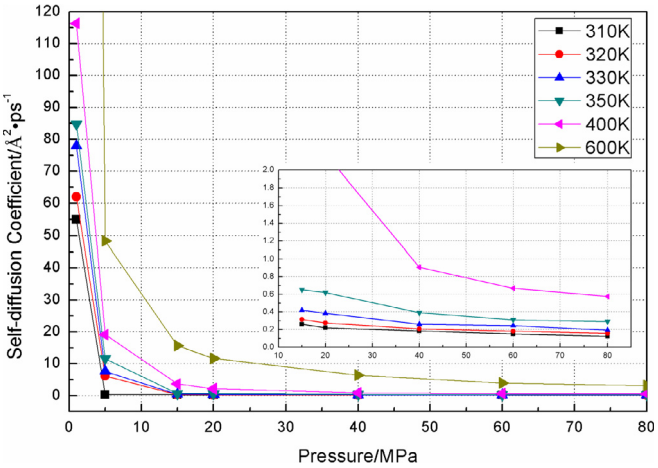

Fig. 8. Self-diffusion coefficients measured by EPM2 model.

region was a little lower than the average. The density difference will reduce if the system average density is high.

And finally, we calculated the thermal conductivity of carbon dioxide at 250 K using EPM2_flex model, Cygan_flex model and TraPPE_flex model. The results are shown in Fig. 11 and Table 4. As the density of the system increases, the pressure of the system increases, which leads to an increase in the thermal conductivity. The result agrees with the NIST data. The relative error in this study is about 4.4%–14.8%. It could be observed that the thermal conductivities calculated from flexible models were higher than the NIST data, this phenomenon is consistent with the reference [10].

4. Conclusions

Supercritical carbon dioxide has some excellent properties, so we investigate the performance of several models of carbon dioxide along liquid-vapor coexist curve and supercritical state, and the results show that they can be used to predict various thermal properties and have acceptable accuracy in a wide range. Besides, the structural properties, the self-diffusion coefficients, and the thermal conductivities of carbon dioxide are obtained. EMP2 and Cygan_flex models are more accurate than the others. Radial distribution functions are in good agreement with X-ray and neutron diffraction experiment results and the short-range structure lose with the increasing temperature. The self-diffusion coefficient would decrease with the increasing pressure and it increases with increasing temperature. The self-diffusion coefficient is close to that of liquid state when carbon dioxide is at supercritical state. The thermal conductivity of carbon dioxide is investigated using non-equilibrium molecular dynamics simulation. We thermostat the temperature of hot and cold regions and probed the heat flux and then calculate the thermal conductivity. The result shows agreement with experiment trend.

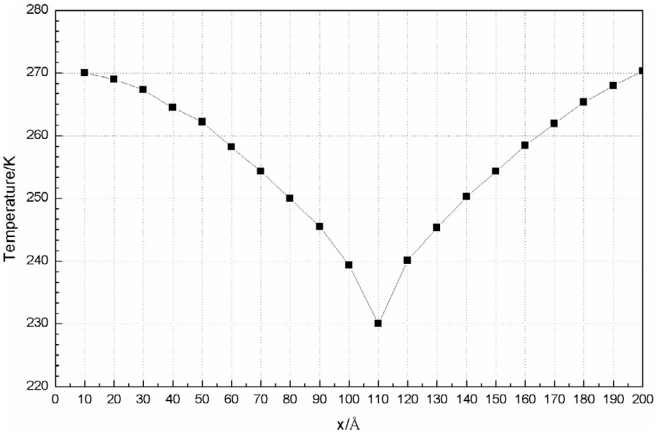

Fig. 9. Temperature distribution along x-direction.

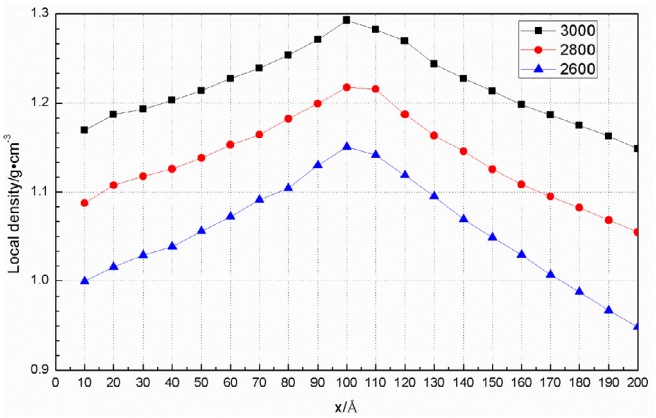

Fig. 10. Density distribution along x-direction.

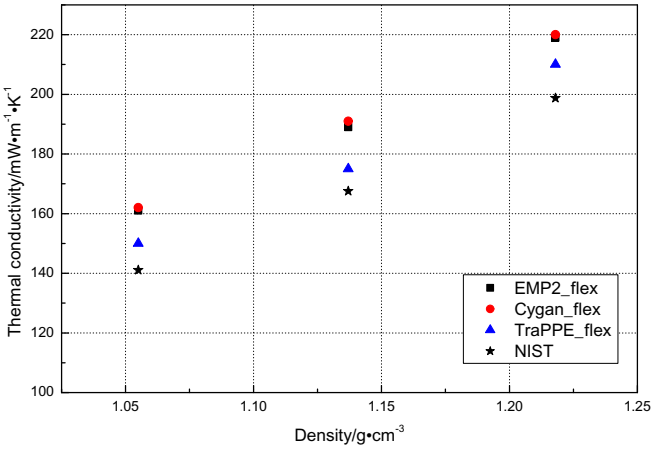

Fig. 11. Calculated thermal conductivity of carbon dioxide at 250 K.

Table 4
Comparison of thermal conductivity ($mW \cdot m^{-1} \cdot K^{-1}$) results obtained by simulation with experimental values.

Density (g·cm-3)	EPM2_flex	Cygan_flex	TraPPE_flex	Expt.
1.055	161.1	162.3	150.4	141.09
1.137	189.3	191.5	175.2	167.53
1.218	219.5	220.3	210.0	198.77

Acknowledgment

This work has been supported by the National Natural Science Foundation of China (Grant number 51876161 and 51506159) and Shaanxi Natural Science Foundation (2017JM5131).

References

[1] Sun EH, Xu JL, Li MJ, Liu GL, Zhu BG. Connected-top-bottom-cycle to cascade utilize flue gas heat for supercritical carbon dioxide coal fired power plant.

Energy Convers Manag 2018;172:138–54.
[2] Ahn Y, Bae SJ, Kim M, Cho SK, Baik S, Lee JI, et al. Review of supercritical co2 power cycle technology and current status of research and development. Nucl Eng Technol 2015;47(6):647–61.
[3] Zhang Y, Zheng X, He MG, Chen YT. Measurement of thermal diffusivity and speed of sound of dibutyl ether from 303.15 K to 688.15 K and up to 7.5 MPa. Fluid Phase Equilib 2016;427:320–7.
[4] Kunz O, Wagner W. The GERG-2008 wide-range equation of state for natural gases and other mixtures: an expansion of GERG-2004. J Chem Eng Data 2012;57(11):3032–91.
[5] Peng DY, Robinson DB. A new two-constant equation of state. Ind Eng Chem Fundam 1976;15(1):59–64.
[6] Bauer BA, Patel S. Properties of water along the liquid-vapor coexistence curve via molecular dynamics simulations using the polarizable TIP4P-QDP-LJ water model. J Chem Phys 2009;131(8):16.
[7] Zhang XB, Liu QL, Zhu AM. An improved fully flexible fixed-point charges model for water from ambient to supercritical condition. Fluid Phase Equilib 2007;262(1–2):210–6.
[8] Wang JM, Hou TJ. Application of molecular dynamics simulations in molecular property prediction 1: density and heat of vaporization. J Chem Theory Comput 2011;7(7):2151–65.
[9] Romer F, Lervik A, Bresme F. Nonequilibrium molecular dynamics simulations of the thermal conductivity of water: a systematic investigation of the SPC/E and TIP4P/2005 models. J Chem Phys 2012;137(7):8.
[10] Trinh TT, Vlugt TJH, Kjelstrup S. Thermal conductivity of carbon dioxide from non-equilibrium molecular dynamics: a systematic study of several common force fields. J Chem Phys 2014;141(13):7.
[11] Stubbs JM. Molecular simulations of supercritical fluid systems. J Supercrit Fluids 2016;108:104–22.
[12] Mayo SL, Olafson BD, Goddard WA. DREIDING: a generic force-field for molecular simulations. J Phys Chem 1990;94(26):8897–909.
[13] Rane KS, Murali S, Errington JR. Monte Carlo simulation methods for computing liquid-vapor saturation properties of model systems. J Chem Theory Comput 2013;9(6):2552–66.
[14] Zhang ZG, Duan ZH. An optimized molecular potential for carbon dioxide. J Chem Phys 2005;122(21):15.
[15] Murthy CS, Singer K, McDonald IR. Interaction site models for carbon-dioxide. Mol Phys 1981;44(1):135–43.
[16] Harris JG, Yung KH. Carbon dioxides liquid-vapor coexistence curve and critical properties as predicted by a simple molecular-model. J Phys Chem 1995;99(31):12021–4.
[17] Potoff JJ, Siepmann JI. Vapor-liquid equilibria of mixtures containing alkanes, carbon dioxide, and nitrogen. AIChE J 2001;47(7):1676–82.
[18] Nieto-Draghi C, de Bruin T, Perez-Pellitero J, Avalos JB, Mackie AD. Thermodynamic and transport properties of carbon dioxide from molecular simulation. J Chem Phys 2007;126(6).
[19] Perez-Blanco ME, Maginn EJ. Molecular dynamics simulations of CO2 at an ionic liquid interface: adsorption, ordering, and interfacial crossing. J Phys Chem B 2010;114(36):11827–37.
[20] Cygan RT, Romanov VN, Myshakin EM. Molecular simulation of carbon dioxide capture by montmorillonite using an accurate and flexible force field. J Phys Chem C 2012;116(24):13079–91.
[21] Aimoli CG, Maginn EJ, Abreu CRA. Force field comparison and thermodynamic property calculation of supercritical CO2 and CH4 using molecular dynamics simulations. Fluid Phase Equilib 2014;368:80–90.
[22] Mezei M. Theoretical calculation of the liquid-vapor coexistence curve of water, chloroform and methanol with the cavity-biased monte-carlo method in the gibbs ensemble. Mol Simul 1992;9(4):257–67.
[23] Fan ZY, Siro T, Harju A. Accelerated molecular dynamics force evaluation on graphics processing units for thermal conductivity calculations. Comput Phys Commun 2013;184(5):1414–25.
[24] MullerPlathe F. A simple nonequilibrium molecular dynamics method for calculating the thermal conductivity. J Chem Phys 1997;106(14):6082–5.
[25] Inzoli I, Simon JM, Kjelstrup S, Bedeaux D. Thermal effects during adsorption of n-butane on a silicalite-1 membrane: a non-equilibrium molecular dynamics study. J Colloid Interface Sci 2007;313(2):563–73.
[26] Okumura H, Yonezawa F. Molecular dynamics study of liquid–vapor coexistence curves and supercritical fluids. Physica B 2001;296:180–3.
[27] Ikeshoji T, Hafskjold B. Nonequilibrium molecular-dynamics calculation of heat-conduction in liquid and through liquid-gas interface. Mol Phys 1994;81(2):251–61.
[28] Chen L, Chen PF, Li ZZ, He YL, Tao WQ. The study on interface characteristics near the metal wall by a molecular dynamics method. Comput Fluids 2018;164:64–72.
[29] Chiappini S, Nardone M, Ricci FP, BellissentFunel MC. Neutron diffraction measurements on high pressure supercritical CO2. Mol Phys 1996;89(4):975–87.
[30] Vantricht JB, Fredrikze H, Vanderlaan J. Neutron-diffraction study of liquid carbon-dioxide at 2-thermodynamic states. Mol Phys 1984;52(1):115–27.
[31] Cipriani P, Nardone M, Ricci FP, Ricci MA. Orientational correlations in liquid and supercritical CO2: neutron diffraction experiments and molecular dynamics simulations. Mol Phys 2001;99(4):301–8.
[32] Cipriani P, Nardone M, Ricci FP. Local orientational correlations in fluid CO2 in a wide range of thermodynamic parameters. Nuovo Cimento Soc Ital Fis D-Condens Matter At Mol Chem Phys Fluids Plasmas Biophys. 1998;20(7–8):1147–52.
[33] Saharay M, Balasubramanian S. Evolution of intermolecular structure and dynamics in supercritical carbon dioxide with pressure: an ab initio molecular dynamics study. J Phys Chem B 2007;111(2):387–92.
[34] Chen L, Tao WQ. Study on diffusion processes of water and proton in pem using molecular dynamics simulation. Physical and Numerical Simulation of Material Processing 2011:1266–72.
[35] Li ZZ, Chen L, Tao WQ. Molecular dynamics simulation of water permeation through the Nafion membrane. Numer Heat Tranf A-Appl. 2016;70(11):1232–41.
[36] Higashi H, Tamura K. Calculation of diffusion coefficient for supercritical carbon dioxide and carbon dioxide plus naphthalene system by molecular dynamics simulation using EPM2 model. Mol Simul 2010;36(10):772–7.
[37] Chen L, Zhang H, Li ZZ, He YL, Tao WQ. Experimental and numerical study on thermal conductivity of proton exchange membrane. J Nanosci Nanotechnol 2015;15(4):3087–91.
[38] Chen L, Huang DB, Wang SY, Nie YN, He YL, Tao WQ. A study on dynamic desorption process of methane in slits. Energy 2019;175:1174–80.
[39] Wang YY, Zhao ZJ, Liu YF, Wang DJ, Ma C, Liu JP. Comprehensive correction of thermal conductivity of moist porous building materials with static moisture distribution and moisture transfer. Energy 2019;176:103–18.
[40] Tang GH, Bi C, Zhao Y, Tao WQ. Thermal transport in nano-porous insulation of aerogel: Factors, models and outlook. Energy 2015;90(1):701–21.
[41] Onyekonwu MO. The effects of relative permeability characteristics and thermal conductivity on in situ combustion performance. Energy 1988;13(8):619–24.
[42] Hopkins PE, Kaehr B, Piekos ES, Dunphy D, Brinker CJ. Minimum thermal conductivity considerations in aerogel thin film. J Appl Phys 2012;111:113532.